Published in final edited form as:
Biochemistry. 2012 July 10; 51(27): 5422–5433. doi:10.1021/bi300598g.

Identification and Characterization of Solvent Filled Channels in Human Ferrochelatase[†,¥]

Amy E. Medlock[*], **Wided Najahi-Missaoui**[§], **Teresa A. Ross**[‡], **Tamara A. Dailey**, **Joseph Burch**, **Jessica R. O'Brien**, **William N. Lanzilotta**, and **Harry A. Dailey**
Biomedical and Health Sciences Institute, Department of Biochemistry and Molecular Biology, Athens, GA 30602, USA

Abstract

Ferrochelatase catalyzes the formation of protoheme from two potentially cytotoxic products, iron and protoporphyrin IX. While much is known from structural and kinetic studies on human ferrochelatase of the dynamic nature of the enzyme during catalysis and the binding of protoporphyrin IX and heme, little is known about how metal is delivered to the active site and how chelation occurs. Analysis of all ferrochelatase structures available to date reveals the existence of several solvent filled channels which originate at the protein surface and continue to the active site. These channels have been proposed to provide a route for substrate entry, water entry and proton exit during the catalytic cycle. In order to begin to understand the functions of these channels, a number of variants which line these solvent filled channels were investigated in vitro and in vivo. Data presented herein support the role of one of these channels, which originates at the surface residue H240, in iron delivery to the active site. Structural studies of the arginyl variant of the conserved residue F337, which resides at the back of the active site pocket, suggest that it not only regulates the opening and closing of active site channels, but also plays a role in regulating the enzyme mechanism. These data provide insight into the movement of substrate and water into and out of the active site and how this movement is coordinated with the reaction mechanism.

Keywords

Heme synthesis; Ferrochelatase; Protoporphyrin IX; X-ray crystallography; Iron; Chelation

Heme is an essential molecule for most organisms and is a cofactor for proteins involved in a number of cellular processes including aerobic respiration, carbohydrate and lipid metabolism, nucleic acid processing, and cellular signaling (1–3). Within eukaryotes the biosynthetic pathway is conserved after the synthesis of the first committed intermediate, 5-aminolevulinate (ALA), while in prokaryotes significant differences are found at several

[†]This research was supported by National Institutes of Health grant DK32303 to (H.A.D.) and National Science Foundation grant MCB0835432 (W.N.L.).

[¥]PDB Accession Codes of the structures reported are H240A 3AQI, F337R 4F4D and F110A/S197C 4F4G.

[*]To whom correspondence should be addressed: Telephone: (706) 542-7843, medlock@uga.edu Fax: (706) 542-5285.
[§]Department of Pharmaceutics and Translational Therapeutics, University of Iowa College of Pharmacy, Iowa City, IA 52242
[‡]Athens Research & Technology, Athens, GA 30601

Supporting Information. Additional figures including the Mg^{2+} ion in the H240A ferrochelatase structure (Figure S1) as well as models of ferrochelatase and protoporphyrinogen oxidase (Figure S2), ferrochelatase and mitoferrin (Figure S3) and ferrochelatase in different conformations (Figure S4) in the membrane can be found in the Supporting Information. Tables summarizing all structures of human ferrochelatase (Table S1) and the validation of Δ*hem15* rescue (Table S2) are also included. This material is available free of charge via the Internet at http://pubs.acs.org.

steps. However, among all organisms, the terminal step of the pathway, chelation of ferrous iron into the protoporphyrin ring by the enzyme ferrochelatase, is conserved. The two best studied ferrochelatase proteins are from the bacterium *Bacillus subtilis* and human. Both of these enzymes have been well characterized kinetically, spectroscopically and structurally. Despite possessing less than ten percent sequence identity, they have highly similar tertiary structure and substrate specificities. The *B. subtilis* protein is a soluble monomer that probably functions in vivo as part of a multienzyme complex (4), while the human enzyme is a homodimer that is associated with the inner mitochondrial membrane (5, 6). Because of the reactive nature of the substrates and product of the ferrochelatase reaction, both substrate entry and product release must be highly coordinated processes in vivo to prevent cytotoxicity. Knowledge of the mechanisms by which this occurs in higher animals is critical to our understanding of diseases resulting from defects in iron, porphyrin and/or heme metabolism.

Based primarily upon structural studies of *B. subtilis* ferrochelatase with and without the bound tight-binding competitive inhibitor *N*-methylmesoporphyrin it was suggested that ferrochelatase functioned as a relatively rigid molecule with an active site mouth within which substrate porphyrin bound and distorted to allow metal insertion (7). However, the determination of the structure of human ferrochelatase with porphyrin substrate bound (8) revealed that the enzyme is quite dynamic and that the “open” active site mouth of the substrate-free enzyme (Figure 1A) closes to tightly bind and distort the porphyrin macrocycle. In this conformation (the so-called “closed” conformation, Figure 1B) the bound porphyrin occupies a spatial position in the enzyme that is distinct from that observed for *N*-methylmesoporphyrin in the *B. subtilis* enzyme (9, 10). The closed conformation has been observed in the substrate bound form of human ferrochelatase and in one subunit of the *Saccharomyces cerevisiae* ferrochelatase (11). Additionally structures of product (heme)-bound enzyme revealed a third conformational variant of human ferrochelatase (the so-called “release” conformation, Figure 1C) (12, 13). In this form, a structurally conserved π helix that forms part of one wall of the active site (14) is found to be partially unwound, extending away from the active site pocket. Consistent with kinetic studies demonstrating that the reaction proceeds in an ordered fashion (15–17) with the slowest step in the reaction being an event occurring after chelation, it has been proposed that the rate-limiting step is most likely product release (18) and involves the unwinding of the π helix (12, 13).

Interestingly, each of the three enzyme conformations (i.e., open, closed and release conformations) possesses a distinct surface contour and surface potential around the mouth region of the enzyme. These catalytically distinct conformational states have been suggested to provide different surfaces upon which multiple protein partners may bind during a complete catalytic cycle (13, 19). Not surprisingly the structural changes observed between the three conformations are not limited to the surface of the protein. The spatial orientation and hydrogen-bonding networks of active site residue side chains have also been observed to vary between the three conformational states (8, 13, 20). Given the extent of the conformational changes that occur upon going from the open to closed, and finally release state, any complete catalytic model must embrace and explain the significant protein structural rearrangements that have been observed.

Ferrochelatase, as an enzyme that is bound to the matrix side of the inner mitochondrial membrane, must obtain both substrates (porphyrin and iron) and release product (heme) across the inner mitochondrial membrane. Hints at how these processes may occur lie in the structural differences seen in the three known conformational states of human ferrochelatase. While conformational changes during catalysis of human ferrochelatase are now well accepted, the fact that all current structures of *B. subtilis* ferrochelatase, including those with the bound inhibitors *N*-methylmesoporphyrin and 2,4-disulfonate-

deuteroporphyrin (9, 10), are of the open (substrate free) form of the enzyme has led to speculation that the bacterial and eukaryotic ferrochelatases somehow differ in their catalytic mechanism (21). However, no structure of the bacterial enzyme with either bound porphyrin substrate or heme has been characterized to date. Of note with respect to the current discussion is the H240A human ferrochelatase structure presented herein (below) in which the presence of a Mg^{2+} atom was observed coordinated via water molecules to several residues of the conserved π helix and a backbone atom of K304 (Figure S1). Mg^{2+} ions in this position have been observed in most *B. subtilis* structures and it is reported to be required for crystal formation of the *B. subtilis* enzyme (22). We suggest that the presence of Mg^{+2} interacting with the π helix probably stabilizes the protein in the open conformation which may explain why only this conformation of the *B. subtilis* enzyme has been observed. A definitive answer to the proposal that the bacterial enzyme operates via a different mechanism from the human enzyme must await the availability of structures of that protein with bound protoporphyrin and product.

In addition to the incomplete understanding of the precise role of many active site residues, information on the mechanism of iron entry as well as steps involved in product exit are lacking. Recent evidence that the mitochondrial inner membrane iron transporter mitoferrin 1 and ferrochelatase physically interact (19) suggests that iron transported across the membrane may be donated directly from mitoferrin 1 to a surface of ferrochelatase. How the iron transits from the outer surface of ferrochelatase to the active site is unknown. However, a recent proposal that the extended π helix may stretch back into the matrix space and pull iron into the active site (21, 23) is clearly untenable given the spatial orientation of human ferrochelatase in the inner mitochondrial membrane. We propose that solvent-filled channels in human ferrochelatase that originate at the surface and terminate in the active site may serve as the entry route for substrate iron and/or as aqueducts which function in substrate binding or product release (20). The work presented herein characterizes several stable solvent-filled channels that exist in human ferrochelatase. Special consideration is given to the side chain of residue F337 since structural data indicates that it is involved in control of the gating of two active site channels as well as in regulating changes in the resting state hydrogen bonding network during catalysis in distinct regions of the active site.

Material and Methods

Mutagenesis, protein expression and purification, and assessment of enzyme activity

All variants were created using the QuikChange® Site-Directed Mutagenesis protocol (Agilent, Santa Clara, CA). Tunnel variants were constructed in the R115L background (5). Two exceptions to this were the F337R variant and the S197C/F110A double variant, which were constructed in the wild-type background. Expression and purification of all variants was carried out as previously described (5, 24, 25). Enzyme activity of each variant was assessed first by rescue of a ferrochelatase deficient strain of *Escherichia coli* (Δ*hemH*) (26, 27). Following rescue of Δ*hemH*, variant ferrochelatases were assayed using the continuous direct spectroscopic method (28).

S. cerevisiae Δhem15 complementation and heme quantitation

All wild-type and variant ferrochelatase genes were cloned into the low-copy yeast shuttle vector pRS316 (gift from W.K. Schmidt, University of Georgia) behind a 350 base pair fragment which contained the *S. cerevisiae* ferrochelatase promoter and targeting sequence. Human ferrochelatase variants were constructed by using the wild-type human ferrochelatase/pRS316 vector as template and QuikChange mutagenesis (Agilent, Santa Clara, CA). The wild-type *S. cerevisiae* strain DY1457 (*MATα*, *ade6*, *can1*, *his3*, *leu2*, *trp1*, *ura3*) and ferrochelatase-deficient strain (*hem15* (29)) (gifts from J. Kaplan and R.J. Crisp,

University of Utah) were utilized. Cells were grown at 30°C with vigorous shaking in complete medium (1% yeast extract, 1% bactopeptone) with 3% glycerol as a carbon source. In the Δ*hem15* strain lacking ferrochelatase-encoded plasmid, media was supplemented with 1.5 mg/ml hemin (Sigma, Saint Louis, MO) made fresh in 0.1 N NaOH and filter-sterilized. Competent Δ*hem15* cells were made and transformed with wild-type and variant ferrochelatase pRS316 constructs using the Frozen-EZ Yeast Transformation II kit (Zymo Research, Orange, CA). Cells were plated and selected on CM-Uracil with 3% glycerol. Whole cell cytochrome content was estimated using a modified version of the previously described pyridine hemochromagen method (30). Yeast cells harboring the ferrochelatase variants were grown and harvested in mid-log phase. Cells were spheroplasted using Zymolyase (MP Biomedicals, Solon, OH). Total protein content of spheroplasts was measured using the BCA assay (Pierce, Rockford, IL). Duplicate samples were used in the hemochromagen assays. The 550 nm peak and the total cellular protein concentration were used to calculate the total amount of cytochromes b + c since they represent the major heme pools.

Crystallization, data collection, model building, refinement and coordinates

Protein for crystallization was prepared as previously described (8, 13). All crystals were grown using the hanging drop method by mixing 2μL of freshly prepared enzyme with an equivalent amount of well solution, followed by incubation at 18°C. The EasyXtal Crystal support (Qiagen, Valencia, CA) was used for crystallization and each well contained 500 μL of precipitating solution. Crystals typically formed in two to five days. Crystals for the H240A variant were obtained using a well solution of 0.2 M magnesium chloride, 0.1 M Bis-Tris pH 6.5 and 25% PEG 3350. Crystals for the F337R and S197C/F110A variants were obtained using precipitating solution containing 0.1 M Bis-Tris pH 6.5, 0.05 M ammonium sulfate and a range of pentaerythritol ethoxylate (15/4 EO/OH) varying from 20% to 35%. The H240A crystals were soaked in a stepwise fashion (2.5 % increments) in mother liquor containing increasing concentrations of glycerol to a final concentration of 15%. In all other cases the crystals could be frozen after increasing the concentration of pentaerythritol ethoxylate (15/4 EO/OH) to 30% in a similar manner.

All data sets for the ferrochelatase crystals were collected at The Advanced Photon Source and SER-CAT on beamline 22-ID. Phases were obtained by using a single monomer of ferrochelatase, taken from the model of the wild-type enzyme (PDB ID 2QD4), as a molecular replacement search model. Molecular replacement was performed using the program CNS (31), version 1.2. Initially the [2Fe-2S] cluster was omitted from the molecular replacement search model so that strong positive peaks in the difference map could be used as indicators of reasonable solutions based on the positions of the iron atoms. Once reasonable solutions were identified for the entire asymmetric unit, CNS was also used to perform rigid body refinement and generate a composite omit map using the simulated annealing protocol. Iterative rounds of model building and refinement were performed with the programs COOT (32) and CNS, respectively. Typically, the backbone and [2Fe-2S] cluster were initially modeled based on the composite omit map and difference maps, and then the side chain atoms, complete with any potential alternate conformations, were modeled before placing water molecules. Data collection and refinement statistics for all structures are listed in Table 1. Coordinates for all structures have been deposited in the RCSB Protein Data Bank and PDB IDs are listed in Table 1. All graphical representations were created using PyMol (33), WinCoot (34) and Caver (35).

Results and Discussion

Ferrochelatase is associated with the matrix side of the mitochondrial inner membrane (6). Since the active site pocket of ferrochelatase opens into the mitochondrial inner membrane,

but does not span the membrane, acquisition of substrates requires the transmembrane transport of both iron and porphyrin. Biochemical data exist to support a model whereby ferrochelatase acquires protoporphyrin directly across the membrane from the previous enzyme, protoporphyrinogen oxidase, via a transient complex (36, 37). In addition, with the availability of crystallographic structures for both ferrochelatase and protoporphyrinogen oxidase, in silico docking exercises demonstrate that such an interaction can occur (38) (Figure S2). No evidence exists to support the transiting of iron via the same route as porphyrin from protoporphryinogen oxidase, and thus another pathway likely exists for ferrochelatase to obtain ferrous iron. Acquisition of substrate iron could occur from a transmembrane transporter via the main opening to the active site pocket of ferrochelatase only if considerable molecular motion, or rocking, of ferrochelatase occurs within the membrane.

Recent data provide support for a model of iron acquisition from the inner mitochondrial membrane iron transporter mitoferrin 1 (19). Mitoferrin 1 is a typical mitochondrial inner membrane solute transporter which spans the membrane, so transported iron will be available on the matrix side of the inner mitochondrial membrane (39) (Figure S3). Hunter and Ferreira (23) have proposed that ferrochelatase may obtain iron from mitoferrin or frataxin via the extended π helix of the enzyme. Iron would then follow a track composed of the conserved acidic residues along the π helix. This suggestion has also been made by others for the *B. subtilis* ferrochelatase in which the helix has not been observed to extend (40). This role of the π helix is not supported by amide hydrogen/deuterium exchange experiments done with human ferrochelatase (41). Two substantial discrepancies between the Hunter and Ferreira model and published data currently exist (23). First, their model is based upon a single monomer, not the homodimer, and spatially misrepresents published data with regard to overall orientation of the native homodimeric protein relative to the membrane (42, 43). The region they cite as the membrane binding surface is, in fact, the dimer interface. Thus, their homodimer would be oriented with one subunit completely submerged in the lipid bilayer and the other completely exposed within the matrix space. All available crystal structures of dimeric human ferrochelatase are consistent with a spatial orientation where the π helix unwinds into the membrane and not back up into the matrix (Figure S4). Secondly, no data exist showing that metal ions bind to residues of the π helix when it is in the unwound state. Indeed, available data suggest that the helix extension is related to heme release, and in the absence of heme there is nothing to stabilize the extended helix. Thus, the model proposed by Hunter and Ferreira (23) would require simultaneous exit of heme and entrance of iron via the same path. In the absence of product release, no substrate iron would bind, which does not fit with overall kinetic analysis (16, 44–46) or structural studies (11–13, 22, 40, 43, 47). We believe that a more reasonable hypothesis is that iron is donated from mitoferrin (or possibly via an as yet unidentified iron chaperone intermediate) directly to a matrix exposed iron portal on the surface of ferrochelatase and then transits to the active site via a solvent filled channel.

Solvent filled channels

Examination of the available crystal structures of wild-type and variants of human ferrochelatase (Table S1) reveals the presence of four solvent filled channels within the protein (Figure 2) that are of sufficient size to accommodate water and/or a desolvated metal ion. In the solved structures, these channels contain well ordered water molecules that show some conservation between species. For the current discussion two channels are named based upon the terminal residue of the channel within the human enzyme (i.e., H240 and Q139). Two additional channels are named for the structures with which they are associated (i.e., cluster channel and dimer interface channel).

Channel H240 is found in the human and *S. cerevisiae* ferrochelatase structures. It is open to the back of the active site pocket when the enzyme is in the open conformation (Figure 2A). Channel Q139 is a shorter channel that is present in the *B. subtilis*, human and *S. cerevisiae* structures. However, in the human enzyme it is open to the active site pocket only with bound porphyrin (closed conformation) (Figure 2B). The cluster channel is a tunnel found in the human enzyme that originates at the protein surface near the opening, or lip, of the active site pocket (at V407) and continues past the [2Fe-2S] cluster. The lip region of the enzyme is proposed to be the portion of the protein which is associated with the inner mitochondrial membrane (43). The cluster channel is absent in *B. subtilis* and *S. cerevisiae* ferrochelatases, which both lack a [2Fe-2S] cluster. Also lacking in the monomeric *B. subtilis*, but present in both human and *S. cerevisiae* ferrochelatase, is an internal channel starting at R298 that spans the dimer interface.

Channel H240—This channel extends from H240 on the matrix-exposed or "back" side of the protein into the active site pocket. The imidazole of H240 forms a flap covering the channel end, but there is no obstruction to this side chain being able to flip aside, thus opening a direct, although torturous, solvent-filled pathway to the active site pocket. In the substrate free form of the enzyme this channel is open to the active site (Figure 2A). However, the channel is gated at the distal end from H240 during the catalytic cycle by the side chain of F337. The tunnel is amphipathic in nature with one side being polar and the other being hydrophobic (Figure 3A). The side chains and backbone atoms of the following residues make up the surface of the H240 channel: F237, H240, I241, Q302, V333, P334, A336, F337, S339, H341, E343, T344, L348, A368, S370 and L371. Located on the surface of the enzyme adjacent to the opening of the H240 channel are residues R366 and E369 (Figure 3B), whose side chains are surface exposed for possible protein interactions.

The H240 channel in the open conformation is sufficiently large to allow for egress of active site water as the porphyrin macrocycle enters the active site and/or the entrance of desolvated ferrous iron substrate. Upon porphyrin binding, the benzyl side chain of F337 moves into a position to close the H240 channel which concomitantly opens channel Q139 to the active site. Following metal insertion and as part of the product release mechanism, the side chain of F337 swings back to reopen channel H240. This may facilitate water re-entry into the active site as the heme product departs. The possibility that the Q139 channel could be a site in which substrate iron is sequestered to be available only when F337 swings to open the channel upon porphyrin binding is possible, but seems unlikely since no structure of ferrochelatase in any conformation has been obtained with a bound iron atom in this channel.

To examine the possibility that the H240 channel serves as an iron portal that obtains substrate iron from a donating partner protein in situ, two sets of experiments were conducted. In the first we examined the impact of mutations of the surface residues R366 and E369, which surround the H240 channel opening on the back side of ferrochelatase (Figure 3B), in vivo by assessing growth and heme production of cells with these variants. In the second, the impact of altering the side chains of channel-lining residues on enzyme activity was determined in vitro.

The in vivo experimental model employed the ferrochelatase deficient *S. cerevisiae* mutant Δ*hem15* (29). R366 and E369 are conserved between human and *S. cerevisiae* ferrochelatases, although there is a conservative replacement of the histidine at 240 in human by glutamine (N212) in the yeast. A low copy number plasmid encoding the *S. cerevisiae* ferrochelatase promoter-regulated wild-type human ferrochelatase complements the Δ*hem15* yeast mutant as well as the plasmid encoded *S. cerevisiae* ferrochelatase (Table S2). This complementation is of note since the human enzyme differs from the *S. cerevisiae*

ferrochelatase in that it possesses a [2Fe-2S] cluster that is essential for activity (48). A number of variant human ferrochelatases were analyzed for their ability to support growth and heme synthesis of Δ*hem15* yeast. Among the enzyme variants examined were some that have previously been shown to have little or no measurable enzyme activity in vitro (Y165L, H263C and R164L/Y165L) (25) and, thus, these served as negative controls. As expected these variants did not support normal growth or heme production of the Δ*hem15* yeast mutant (Table 2).

The H240 channel openings are on either side of the homodimeric ferrochelatase as it is proposed to sit on the membrane thus placing them in a position that is spatially close to where one might expect an adjacent mitoferrin molecule to be (Figures 4A, 4B and S3). To investigate the possibility that the H240 channel has a role in substrate iron acquisition we created variants in which the imidazole side chain of H240 was replaced with either a smaller, uncharged alanine (H240A) or acidic side chain (H240E). Interestingly the H240A variant-expressing Δ*hem15* had close to normal heme synthesis while the H240E variant had significantly reduced cellular heme levels (Table 2). Because R336 and E369 are surface located residues in close proximity to H240 and might be involved in complementary charge pair interactions with an interacting, iron supply protein, we created the H240A/R366E and H240A/E369T variants. When these double variants of H240A/R366E and H240A/E369T were expressed in Δ*hem15*, reduced amounts of heme were synthesized. These data are consistent with the hypothesis that the matrix surface of the H240 channel is involved in obtaining iron from a donor protein.

To ensure that the H240A mutation did not have an impact on the overall structure and/or orientation of active site residues, the H240A variant was crystallized and its structure solved to 1.8 Å. This variant revealed a structure very similar to the open conformation of the wild-type enzyme and R115L variant with a root mean square deviation (RMSD) between the Cα atoms of 0.358 Å, as well as similar orientation of most amino acid side chains. One difference observed in the H240A structure is the presence of a Mg^{2+} atom coordinated via water molecules to several residues of the conserved π helix (E347, Y352, E351) and the backbone atoms of K304 (Figure S1).

In addition, a selection of surface variants on the back side of the enzyme distant from H240 which have previously been reported to bind cobalt (H231A/D383A and H231A/D383K) (43) (Figure 4A and B) were examined. Assuming that the charged surface residues at the cobalt-binding site were essential for metal binding and by eliminating these charges the affinity of the enzyme for substrate metal would be significantly diminished, we created variants in which the charges of the putative metal-binding residues were eliminated (H231A/D383A), or altered by changing the acidic glutamate to a basic lysine (H231A/D383K). None of these alterations had any significant impact on the ability of Δ*hem15* cells to produce heme suggesting that the previously identified cobalt-binding site (43) is not necessary for normal iron delivery.

It has also been proposed by some that the small mitochondrial matrix iron-binding protein frataxin is responsible for iron delivery to ferrochelatase (50). The surface residues R290 and E289 have been suggested to provide putative docking site on ferrochelatase for iron delivery from frataxin. Thus, we individually changed the charge of both residues (R290E and E289K) and collectively eliminated the side chain charge of both residues (E289A/R290A) assuming that such alterations would diminish or abolish the affinity of ferrochelatase for frataxin. None of these variants resulted in a significant phenotype in the complemented Δ*hem15* yeast cells (Table 2). This suggests that if frataxin serves as an iron donor, it is not via this site.

If the H240 channel is an iron portal, one would expect that alteration of the residues lining the tunnel would have an impact on enzyme activity. Thus, a number of H240 channel variants were purified and characterized. For these variants the ability to complement the ferrochelatase-lacking *E. coli* Δ*hemH* along with kinetic parameters for purified enzyme were examined (Table 3). For two variants individual polar side chains contributing to the surface of the channel were replaced by alanine (Q302A and S370A). In one instance the polar uncharged side chain of residue S370 was replaced by cysteine, a potentially strong iron ligand. All three variants (Q302A, S370A and S370C) exhibited an increased K_m for iron. The variants F237Y and A368L which introduced modest alterations in side chain polarity or size showed decreases in k_{cat}. A similar result was found for the P334L variant. Two more drastic variants, F337R and T344K, lacked measurable enzyme activity and did not complement the *E. coli* Δ*hemH* mutant. Interestingly, T344 is also a component of the conserved π helix and is located close to residue H341 (below). The change in size and charge that occurs in the T344K variant may allow it to interact with H341 resulting in the reorientation of H341 and thus loss of activity.

Unfortunately, indisputable designation of the H240 channel as a conduit for substrate iron based upon in vitro assays is problematic. Even if the H240 channel is the natural iron portal, it is reasonable to assume that variants with a partial or completely blocked channel may still have some measurable in vitro activity that would be attributable to iron diffusing into the mouth of the active site in the enzyme assay. Given that channel variants have no impact on overall enzyme structure and, with the exception of F337, are not located within the active site pocket, any enzyme activity diminution would be expected to result from an inability of the channel to provide its normal function. Variants completely lacking activity could thus represent enzymes in which the mutation disrupts the normal catalytic cycle. As discussed below, we posit that this is what occurs in the F337R variant.

Channel Q139—A shorter channel that is present in all published ferrochelatase structures is the Q139 channel. In the wild-type human enzyme the Q139 channel is open to the active site only in the closed (substrate bound) conformation (8, 13). However, in structures in which the active site hydrogen bonding network has been disrupted, such as has been reported to occur for the variants possessing the mutations H263C or H341C, and in the F337A variant where the physical barrier attributable to the F337 side chain is missing, the Q139 channel is open to the active site pocket (20). Residues found to line channel Q139 are N75, I132, T136, Q139, F163, Q190, F337 and T338.

To investigate potential roles that residues lining the Q139 channel may play, enzyme variants possessing I132A and Q139A/L were constructed and their activity assessed by rescue of *E. coli* Δ*hemH* (Table 3). All of these variants possessed enzyme activity sufficient to rescue the Δ*hemH* mutant. To further investigate the Q139L variant, in vitro assays were performed (Table 3). This variant possessed a significantly diminished k_{cat}. The F337A and N75A variants of human ferrochelatase, which were produced and analyzed in previous studies, also possess decreased k_{cat} (20). The diminished enzyme activity of F337A is of note since its structure is very similar to that of the wild-type enzyme with an intact open conformation hydrogen bond network. The only substantial difference between the wild-type enzyme and F337A variant is that both the H240 and Q139 channels are simultaneously open to the active site in the variant. N75 is of interest since previous and current studies suggest that it bridges the hydrogen bond networks found in the upper and lower active site pocket (see below and (20)).

It is of note, that an equivalent to the human Q139 channel is observed in the *B. subtilis* ferrochelatase structures. This channel is continuous with the active site pocket and also open at the protein surface in most structures (9, 10, 22, 40, 47, 51, 52). Analysis of the

alanine variants of the equivalent of Q139 (residue Q63 in *B. subtilis*) showed decreased in vitro activity yet unchanged in vivo activity as assessed by growth measurements (53). From the results presented herein as well as the *B. subtilis* studies the role of the Q139 channel in the catalytic mechanism is unclear.

Cluster channel—The cluster channel originates at the active site lip region at residue V407, passes by the [2Fe-2S] cluster and ends just short of the dimer interface channel at residue R298 (Figure 5). Interestingly, it is the guanido side chain of R298 from the B subunit that intercalates into the A subunit thereby blocking the A subunit cluster channel from the dimer interface channel (below) and vice-a-versa. The cluster channel and its opening are lined by the residues D95, D97, L98, Y194, C196, S197, G199, S201, L203, N204, R226, R272, Q398, L399, S402, C403, C406, V407, N408, C411, T414, and K415. Four of these residues (C196, C403, C406 and C411) are the coordinating residues for the [2Fe-2S] cluster which forms a portion of one wall of the channel.

Only one residue in the cluster channel was investigated and the kinetic parameters for the S201A (inside the channel across from the cluster) variants are shown in Table 3. This variant possessed diminished K_ms and k_{cat}. Given that this residue also has access to the active site pocket, it may play a role in the hydrogen bonding network.

The structure of the F110A/S197C variant was solved to 2.6 Å. The structure of this variant is very similar to the open conformation with minimal differences in the orientation of side chain residues for most amino acids (RMSD Cα atoms of 0.448 Å). This double variant rescued *E. coli* Δ*hemH*, although kinetic parameters were not determined. Given its position and the fact that the *S. cerevisiae* ferrochelatase lacks a [2Fe-2S] cluster, it would appear unlikely that the cluster channel is directly involved in iron acquisition. However, for ferrochelatases that possess the cluster, this channel, which provides an aqueous channel to the cluster, may play some role in catalysis or regulation of activity.

Dimer interface channel—The dimer interface channel is formed between the interface of the two ferrochelatase monomers (A and B). Interestingly the channel structure is conserved between the human and *S. cerevisiae* ferrochelatases despite the significant lack of residue homology between these two proteins at the dimer interface. The channel is lined by identical residue participants from both subunits, including V270, D274, P275, P277, Q278, E279, S281, Y297, R298, L299, W301, L311, G312, P313 and Q398 (Figure 6). Thus, it possesses two-fold symmetry with regard to charge distribution. In the crystal structures this channel is closed at both ends. The channel is separated from the end of the cluster channel (A subunit) by the side chains of R298 (of the B subunit) and Q398 (of the A subunit). Access from the channel to the enzyme surface is only blocked by the hydroxyl group of Y297 (of the B subunit) and the carboxyl group of E279 (of the A subunit). One could imagine that with minimal molecular movement the channel could open to the protein surface and/or the cluster channels. Thus it is not surprising that in some structures one finds a glycerol molecule in this channel (12), indicating that sufficient molecular mobility exists to allow for access of small molecules present in the crystallization solvent to this interior channel. Since this channel does not have access to the active site, a role for this channel in substrate delivery is not readily apparent.

Channel gating by F337 and its relationship to the catalytic cycle

F337 is a conserved residue located at the back side of the active site pocket. Structural data from human ferrochelatase demonstrates that the orientation of the benzyl ring of F337 determines whether the H240 or Q139 channels are open to the active site pocket. It is of note that F337 is part of a loop that connects β strand 7 and the π helix. Thus, rotation of

F337 has the potential to influence and/or be influenced by the secondary structure of this region.

In an effort to understand what may control the movement of F337 and determine if it serves solely as a gate keeper or has additional functions during catalysis, the structure and function of two ferrochelatase variants were investigated. In one the benzyl side chain was replaced with the spatially smaller methyl group of alanine (F337A), and in another it was replaced by a bulky, charged guanido of arginine (F337R). The previously described F337A variant does not have any alterations in the resting state hydrogen bond network in the active site, but exhibits a five-fold reduction in k_{cat} (20). Thus, the benzyl group and/or the ability to gate the H240 and Q139 channels are not essential for enzyme activity, but in its absence the activity of ferrochelatase is significantly impaired.

The F337R variant was constructed, expressed and characterized. The F337R variant has no detectable catalytic activity and does not purify or crystallize with bound substrate or product as is typical of wild type human ferrochelatase. The structure of this variant was determined to 1.8 Å. This variant possesses an open conformation with cholate molecules present in each active site as well as in the entry route to the active site as is observed for the wild-type human ferrochelatase in the open conformation. However, in the F337R variant enzyme one of the active site cholate molecules is rotated 180° compared to its position in the active site of the open conformation wild-type (2QD3 (13)) and R115L variant ferrochelatases (2HRC (8)). This would indicate that the overall surface potential within the active site of the F337R variant is altered from that found in the wild-type protein, which could alter substrate binding. Also of note is the likelihood that the H240 and/or Q139 channels are blocked at their entrance to the active site by the F337R side chain thereby preventing iron entry and/or water movement through the channel.

When examining the two subunits (“A” and “B”) of the homodimeric F337R variant human ferrochelatase, the orientations of the guanido side chains of residue 337 differ between the A vs B subunits. In the A monomer the side chain of R337 is best modeled in a single orientation with 100% occupancy. However, in the B monomer the guinado group is best modeled in 2 orientations, each with 50% occupancy (e.g. B1 and B2) (Figure 7). One of these two orientations (B1) is identical to what is observed in the A monomer at all times. In this orientation the A and B1 R337 guanido group is within hydrogen bonding distance of the side chains of residues H263, H341 and E343 (Figure 7A). H341 and E343 comprise part of the catalytically important π helix. Hydrogen bonding between the R337 guanido group in this conformation with the imidazole of H341explains the observed 90° rotation of H341 away from what is seen in the wild-type enzyme (Figure 7A). In this orientation H341 can no longer participate in the hydrogen bonding network found in the wild-type open conformation, but instead forms a hydrogen bond with a backbone amine group of the amino terminus of the π helix. In structure models of the B2 monomer, the guanido side chain is within hydrogen bonding distance of N75 at the top of the active site pocket (Figure 7B). As a result, the position and orientation of N75 is distinctly different from that found in both subunits of the wild-type enzyme, and in the A subunit model of the F337R variant. In addition, and only in the B monomer, residue M76, also at the top of the active site pocket opposite H263, is found in three distinct conformations. In one of the M76 side chain conformations (50% occupancy) the side chain is closer to the imidazole side chain of H341 than one finds in the wild type enzyme structure.

The changes in active site pocket residue side chain conformations and the hydrogen bond network observed in the structure of the F337R variant may provide some insight into the catalytic cycle. If one considers a model where iron transits past F337 in its route to chelation, then replacement of the benzyl side chain with the positively charged guanido

side chain in the F337R variant may mimic the presence of the ferrous iron dication at this position. Thus the altered conformations seen in the variant may represent a snapshot of an intermediate stage of the catalytic cycle. The observation of multiple spatial conformations within the active site of the F337R variant would be consistent with the transient interactions of the iron atom as it moves into position for chelation. Additionally, the spatial reorientation of H341 (above) that includes new hydrogen bonds with backbone atoms of the π helix will affect several steps in catalysis including proton abstraction and product release.

Overall, the available data support a role for F337 that is more than a simple gate keeper to the H240 and Q139 channels. The F337R variant structure, in which the hydrogen bond network in the top of the active site is altered depending on the conformation of residue F337R, and in the bottom of the active site pocket is partially disrupted by the altered conformation of H341, suggests that this residue may help coordinate structural changes between the top and bottom of the active site and modulate the stability of the π helix during the catalytic cycle.

Conclusions

The means by which iron is transported to residues in the active site of human ferrochelatase and the precise residues involved in active site iron binding remain unanswered questions. At the present time the only universal point of agreement appears to be that in vivo ferrous iron and protoporphyrin IX will be delivered directly to ferrochelatase, as both of these substrates are potentially toxic to the cell. For higher organisms containing a ferrochelatase whose active site faces the inner mitochondrial membrane, the mechanism of substrate delivery as well as the release of heme becomes substantially more complex. A reasonable solution to delivering protoporphyrin IX can be found in the proposed transient protein-protein complex formed between protoporphyrinogen oxidase and ferrochelatase (36–38), but the delivery of the ferrous iron must involve additional steps that include desolvation of the hydrated ion. One possible mechanism that has not been explored is the role of enzyme channels to desolvate as well as deliver the metal ion from carriers to the active site. Specifically, the existence of several water filled channels which originate in the active site and end at the protein surface could provide a sheltered conduit by which the redox active ferrous iron substrate could enter from the matrix side of the mitochondrial membrane and move to the active site without exposure to the bulk medium. Such access would allow donation of iron either directly from a membrane spanning transporter (mitoferrin (19)) or a matrix protein without exposing the reactive ferrous iron to the matrix environment. Movement of substrate iron into the active site in this way could provide a means by which metal entry into the active site is regulated in order to control the ordered reaction catalyzed by ferrochelatase.

Data provided herein support the role of the H240 channel in iron delivery. In addition, the channel could also serve as an aqueduct for entry and exit of water molecules from the active site in order to facilitate substrate binding of both protoporphyrin and iron, and product release. These types of aqueducts have been observed in cytochrome P450 enzymes and are thought to contribute to substrate binding and water mediated proton release (54, 55). Evidence for the cluster channel as an aqueduct is supported by hydrogen/deuterium exchange studies in the presence of iron (41). It is possible and likely that the ferrochelatase channels could serve multiple roles and would likely contribute to the regulation of the catalytic mechanism.

The residue F337 which lies at the convergence of the Q139 and H240 channels in the active site is one of the few conserved residues in all ferrochelatases. Both kinetic and structural studies (current and (20)) have suggested that this residue serves as a channel gate and plays

a role in regulating the overall reaction mechanisms. We propose the following model for the role of F337. In the open conformation with the resting hydrogen bond network intact, F337 sits above H341 which serves as a cap to the functionally important π helix. Upon the binding of the porphryin substrate and formation of the closed conformation, F337 reorients and leads to the partial disruption of the resting state hydrogen bond network and the initial destabilization of the π helix. The movement of F337 during the catalytic cycle would likely result in changes in the active site electrostatics, and thus be the impetus for the observed movement of the 6 propionate during the catalytic cycle. While heme propionates have been shown in hemoproteins to be important in binding, orienting and modulating electronic properties (56), ferrochelatase may use changes in the electronic properties of its active site to influence the orientation of the heme propionates and facilitate product release. Following chelation and proton abstraction by H263 and E343, the concomitant disruption of the hydrogen bond network destabilizes the π helix allowing for it to unwind for product release. These proposed roles of F337 are consistent with the data presented herein as well as previous studies (20).

Supplementary Material

Refer to Web version on PubMed Central for supplementary material.

Acknowledgments

The authors thank Dr. Walter K. Schmidt (Univeristy of Georgia) for providing the yeast shuttle vector, Drs. Jerry Kaplan and R. J. Crisp (University of Utah) for providing the Δ*hem15* and wild-type *S. cerevisiase* strains as well as expert advice on the in vivo experiments, Amy E. Burden for preparation of several human ferrochelatase variants and Mrs. Michael Carter and Michael Kassin who worked on crystal growth of the F337R variant.

References

1. Burris TP. Nuclear hormone receptors for heme: REV-ERBalpha and REV-ERBbeta are ligand-regulated components of the mammalian clock. Mol Endocrinol. 2008; 22:1509–1520. [PubMed: 18218725]
2. Faller M, Matsunaga M, Yin S, Loo JA, Guo F. Heme is involved in microRNA processing. Nat Struct Mol Biol. 2007; 14:23–29. [PubMed: 17159994]
3. Mense SM, Zhang L. Heme: a versatile signaling molecule controlling the activities of diverse regulators ranging from transcription factors to MAP kinases. Cell Res. 2006; 16:681–692. [PubMed: 16894358]
4. Dailey TA, Boynton TO, Albetel AN, Gerdes S, Johnson MK, Dailey HA. Discovery and Characterization of HemQ: an essential heme biosynthetic pathway component. J Biol Chem. 2010; 285:25978–25986. [PubMed: 20543190]
5. Burden AE, Wu C, Dailey TA, Busch JL, Dhawan IK, Rose JP, Wang B, Dailey HA. Human ferrochelatase: crystallization, characterization of the [2Fe-2S] cluster and determination that the enzyme is a homodimer. Biochim Biophys Acta. 1999; 1435:191–197. [PubMed: 10561552]
6. Harbin BM, Dailey HA. Orientation of ferrochelatase in bovine liver mitochondria. Biochemistry. 1985; 24:366–370. [PubMed: 3884041]
7. Al-Karadaghi S, Franco R, Hansson M, Shelnutt JA, Isaya G, Ferreira GC. Chelatases: distort to select? Trends Biochem Sci. 2006; 31:135–142. [PubMed: 16469498]
8. Medlock A, Swartz L, Dailey TA, Dailey HA, Lanzilotta WN. Substrate interactions with human ferrochelatase. Proc Natl Acad Sci U S A. 2007; 104:1789–1793. [PubMed: 17261801]
9. Karlberg T, Hansson MD, Yengo RK, Johansson R, Thorvaldsen HO, Ferreira GC, Hansson M, Al-Karadaghi S. Porphyrin binding and distortion and substrate specificity in the ferrochelatase reaction: the role of active site residues. J Mol Biol. 2008; 378:1074–1083. [PubMed: 18423489]
10. Lecerof D, Fodje M, Hansson A, Hansson M, Al-Karadaghi S. Structural and mechanistic basis of porphyrin metallation by ferrochelatase. J Mol Biol. 2000; 297:221–232. [PubMed: 10704318]

11. Karlberg T, Lecerof D, Gora M, Silvegren G, Labbe-Bois R, Hansson M, Al-Karadaghi S. Metal binding to *Saccharomyces cerevisiae* ferrochelatase. Biochemistry. 2002; 41:13499–13506. [PubMed: 12427010]
12. Medlock AE, Carter M, Dailey TA, Dailey HA, Lanzilotta WN. Product release rather than chelation determines metal specificity for ferrochelatase. J Mol Biol. 2009; 393:308–319. [PubMed: 19703464]
13. Medlock AE, Dailey TA, Ross TA, Dailey HA, Lanzilotta WN. A pi-helix switch selective for porphyrin deprotonation and product release in human ferrochelatase. J Mol Biol. 2007; 373:1006–1016. [PubMed: 17884090]
14. Fodje MN, Al-Karadaghi S. Occurrence, conformational features and amino acid propensities for the pi-helix. Protein Eng. 2002; 15:353–358. [PubMed: 12034854]
15. Dailey HA, Fleming JE. Bovine ferrochelatase. Kinetic analysis of inhibition by N-methylprotoporphyrin, manganese, and heme. J Biol Chem. 1983; 258:11453–11459. [PubMed: 6688622]
16. Davidson RE, Chesters CJ, Reid JD. Metal ion selectivity and substrate inhibition in the metal ion chelation catalyzed by human ferrochelatase. J Biol Chem. 2009; 284:33795–33799. [PubMed: 19767646]
17. Hunter GA, Sampson MP, Ferreira GC. Metal ion substrate inhibition of ferrochelatase. J Biol Chem. 2008; 283:23685–23691. [PubMed: 18593702]
18. Hoggins M, Dailey HA, Hunter CN, Reid JD. Direct measurement of metal ion chelation in the active site of human ferrochelatase. Biochemistry. 2007; 46:8121–8127. [PubMed: 17566985]
19. Chen W, Dailey HA, Paw BH. Ferrochelatase forms an oligomeric complex with mitoferrin-1 and Abcb10 for erythroid heme biosynthesis. Blood. 2010; 116:628–630. [PubMed: 20427704]
20. Dailey HA, Wu CK, Horanyi P, Medlock AE, Najahi-Missaoui W, Burden AE, Dailey TA, Rose J. Altered orientation of active site residues in variants of human ferrochelatase. Evidence for a hydrogen bond network involved in catalysis. Biochemistry. 2007; 46:7973–7979. [PubMed: 17567154]
21. Hunter GA, Al-Karadaghi S, Ferreira GC. Ferrochelatase: The Convergence of the Porphyrin Biosynthesis and Iron Transport Pathways. J Porphyr Phthalocyanines. 2011; 15:350–356. [PubMed: 21852895]
22. Hansson MD, Karlberg T, Soderberg CA, Rajan S, Warren MJ, Al-Karadaghi S, Rigby SE, Hansson M. Bacterial ferrochelatase turns human: Tyr13 determines the apparent metal specificity of *Bacillus subtilis* ferrochelatase. J Biol Inorg Chem. 2011; 16:235–242. [PubMed: 21052751]
23. Hunter GA, Ferreira GC. Identification and characterization of an inhibitory metal ion-binding site in ferrochelatase. J Biol Chem. 2010; 285:41836–41842. [PubMed: 20966079]
24. Mayer MR, Dailey TA, Baucom CM, Supernak JL, Grady MC, Hawk HE, Dailey HA. Expression of human proteins at the Southeast Collaboratory for Structural Genomics. J Struct Funct Genomics. 2004; 5:159–165. [PubMed: 15263854]
25. Sellers VM, Wu CK, Dailey TA, Dailey HA. Human ferrochelatase: characterization of substrate-iron binding and proton-abstracting residues. Biochemistry. 2001; 40:9821–9827. [PubMed: 11502175]
26. Frustaci JM, O'Brian MR. Characterization of a *Bradyrhizobium japonicum* ferrochelatase mutant and isolation of the *hemH* gene. J Bacteriol. 1992; 174:4223–4229. [PubMed: 1624416]
27. Miyamoto K, Nakahigashi K, Nishimura K, Inokuchi H. Isolation and characterization of visible light-sensitive mutants of *Escherichia coli* K12. J Mol Biol. 1991; 219:393–398. [PubMed: 2051480]
28. Najahi-Missaoui W, Dailey HA. Production and characterization of erythropoietic protoporphyric heterodimeric ferrochelatases. Blood. 2005; 106:1098–1104. [PubMed: 15831704]
29. Gora M, Grzybowska E, Rytka J, Labbe-Bois R. Probing the active-site residues in *Saccharomyces cerevisiae* ferrochelatase by directed mutagenesis. In vivo and in vitro analyses. J Biol Chem. 1996; 271:11810–11816. [PubMed: 8662602]
30. Berry EA, Trumpower BL. Simultaneous determination of hemes a, b, and c from pyridine hemochrome spectra. Anal Biochem. 1987; 161:1–15. [PubMed: 3578775]

31. Brunger AT. Version 1.2 of the Crystallography and NMR system. Nat Protoc. 2007; 2:2728–2733. [PubMed: 18007608]
32. Emsley P, Lohkamp B, Scott WG, Cowtan K. Features and development of Coot. Acta Crystallogr D Biol Crystallogr. 2010; 66:486–501. [PubMed: 20383002]
33. The PyMOL Molecular Graphics System. Schrödinger, LLC; Version 1.3 ed
34. Emsley P, Cowtan K. Coot: model-building tools for molecular graphics. Acta Crystallogr D Biol Crystallogr. 2004; D60:2126–2132. [PubMed: 15572765]
35. Chovancová, E.; Pavelka, A.; Beneš, P.; Strnad, O.; Brezovský, J.; Kozlíková, B.; Gora, A.; Šustr, V.; Klvaga, M.; Medek, P.; Biedermannová, L.; Sochor, J.; Damborský, J. CAVER 3.0: A Tool for the Analysis of Transport Pathways in Dynamic Protein Structures. (In preparation)
36. Ferreira GC, Andrew TL, Karr SW, Dailey HA. Organization of the terminal two enzymes of the heme biosynthetic pathway. Orientation of protoporphyrinogen oxidase and evidence for a membrane complex. J Biol Chem. 1988; 263:3835–3839. [PubMed: 3346226]
37. Proulx KL, Woodard SI, Dailey HA. In situ conversion of coproporphyrinogen to heme by murine mitochondria: terminal steps of the heme biosynthetic pathway. Protein Sci. 1993; 2:1092–1098. [PubMed: 8358292]
38. Koch M, Breithaupt C, Kiefersauer R, Freigang J, Huber R, Messerschmidt A. Crystal structure of protoporphyrinogen IX oxidase: a key enzyme in haem and chlorophyll biosynthesis. EMBO J. 2004; 23:1720–1728. [PubMed: 15057273]
39. Shaw GC, Cope JJ, Li L, Corson K, Hersey C, Ackermann GE, Gwynn B, Lambert AJ, Wingert RA, Traver D, Trede NS, Barut BA, Zhou Y, Minet E, Donovan A, Brownlie A, Balzan R, Weiss MJ, Peters LL, Kaplan J, Zon LI, Paw BH. Mitoferrin is essential for erythroid iron assimilation. Nature. 2006; 440:96–100. [PubMed: 16511496]
40. Hansson MD, Karlberg T, Rahardja MA, Al-Karadaghi S, Hansson M. Amino acid residues His183 and Glu264 in *Bacillus subtilis* ferrochelatase direct and facilitate the insertion of metal ion into protoporphyrin IX. Biochemistry. 2007; 46:87–94. [PubMed: 17198378]
41. Asuru AP, Busenlehner LS. Analysis of human ferrochelatase iron binding via amide hydrogen/deuterium exchange mass spectrometry. Int J Mass Spectrom. 2011; 302:76–84.
42. Dailey, HA.; Dailey, TA. Ferrochelatase. In: Kadish, KM.; Smith, KM.; Guilard, R., editors. The Porphyrin Handbook. Academic Press; San Diego: 2003. p. 93-122.
43. Wu CK, Dailey HA, Rose JP, Burden A, Sellers VM, Wang BC. The 2.0 A structure of human ferrochelatase, the terminal enzyme of heme biosynthesis. Nat Struct Biol. 2001; 8:156–160. [PubMed: 11175906]
44. Dailey HA. Metal inhibition of ferrochelatase. Ann N Y Acad Sci. 1987; 514:81–86. [PubMed: 3442391]
45. Dailey HA Jr, Lascelles J. Ferrochelatase activity in wild-type and mutant strains of *Spirillum itersonii* Solubilization with chaotropic reagents. Arch Biochem Biophys. 1974; 160:523–529. [PubMed: 4364772]
46. Gaertner RR, Hollebone BR. The in vitro inhibition of hepatic ferrochelatase by divalent lead and other soft metal ions. Can J Biochem Cell Biol. 1983; 61:214–222. [PubMed: 6850416]
47. Lecerof D, Fodje MN, Alvarez Leon R, Olsson U, Hansson A, Sigfridsson E, Ryde U, Hansson M, Al-Karadaghi S. Metal binding to *Bacillus subtilis* ferrochelatase and interaction between metal sites. J Biol Inorg Chem. 2003; 8:452–458. [PubMed: 12761666]
48. Dailey HA, Finnegan MG, Johnson MK. Human ferrochelatase is an iron-sulfur protein. Biochemistry. 1994; 33:403–407. [PubMed: 8286370]
49. Domanski J, Stansfeld PJ, Sansom MS, Beckstein O. Lipidbook: a public repository for force-field parameters used in membrane simulations. J Membr Biol. 2010; 236:255–258. [PubMed: 20700585]
50. Yoon T, Cowan JA. Frataxin-mediated iron delivery to ferrochelatase in the final step of heme biosynthesis. J Biol Chem. 2004; 279:25943–25946. [PubMed: 15123683]
51. Al-Karadaghi S, Hansson M, Nikonov S, Jonsson B, Hederstedt L. Crystal structure of ferrochelatase: the terminal enzyme in heme biosynthesis. Structure. 1997; 5:1501–1510. [PubMed: 9384565]

52. Shipovskov S, Karlberg T, Fodje M, Hansson MD, Ferreira GC, Hansson M, Reimann CT, Al-Karadaghi S. Metallation of the transition-state inhibitor N-methyl mesoporphyrin by ferrochelatase: implications for the catalytic reaction mechanism. J Mol Biol. 2005; 352:1081–1090. [PubMed: 16140324]

53. Olsson U, Billberg A, Sjovall S, Al-Karadaghi S, Hansson M. In vivo and in vitro studies of Bacillus subtilis ferrochelatase mutants suggest substrate channeling in the heme biosynthesis pathway. J Bacteriol. 2002; 184:4018–4024. [PubMed: 12081974]

54. Fishelovitch D, Shaik S, Wolfson HJ, Nussinov R. How does the reductase help to regulate the catalytic cycle of cytochrome P450 3A4 using the conserved water channel? J Phys Chem B. 2010; 114:5964–5970. [PubMed: 20387782]

55. Oprea TI, Hummer G, Garcia AE. Identification of a functional water channel in cytochrome P450 enzymes. Proc Natl Acad Sci U S A. 1997; 94:2133–2138. [PubMed: 9122160]

56. Guallar V, Olsen B. The role of the heme propionates in heme biochemistry. J Inorg Biochem. 2006; 100:755–760. [PubMed: 16513175]

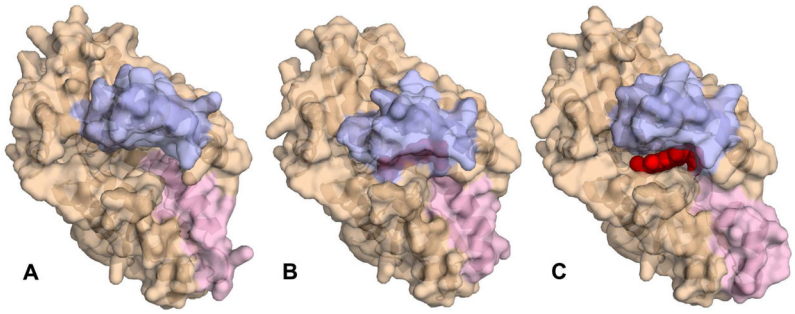

Figure 1. Surface and cartoon representations of the three conformations observed for the human ferrochelatase dimer

Panel A shows the open conformation as observed in the R115L variant (PDB ID 2HRC), panel B shows the closed conformation as observed in the substrate bound E343K variant (PDB ID 2QD1) and panel C shows the release conformation from the heme bound F110A variant (PDB ID 2QD2). The bound porphyrin and heme are shown in the active site as spheres. The surface of the upper lip region is highlighted in purple and the π helix in pink.

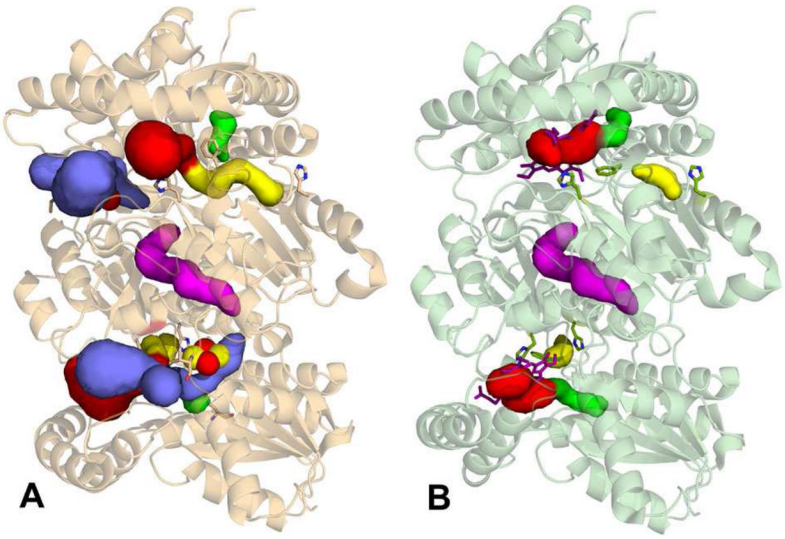

Figure 2. Human ferrochelatase channels

Panel A shows all channels present in the open conformation (PDB ID 2HRC). The channels are colored as follows: H240 yellow, Q139 green, cluster blue and dimer interface magenta. The active site pocket is highlighted in red and is continuous with the H240 channel in the open conformation. Panel B shows the H240, Q139 and dimer interface channels in the closed conformation (PDB ID 2QD1). The bound protoporphyrin IX is shown as purple sticks and the active site pocket is highlighted in red. The Q139 channel is continuous with the active site in the closed conformation. The side chains of residues H240, H263 and F337 are shown as sticks in each panel.

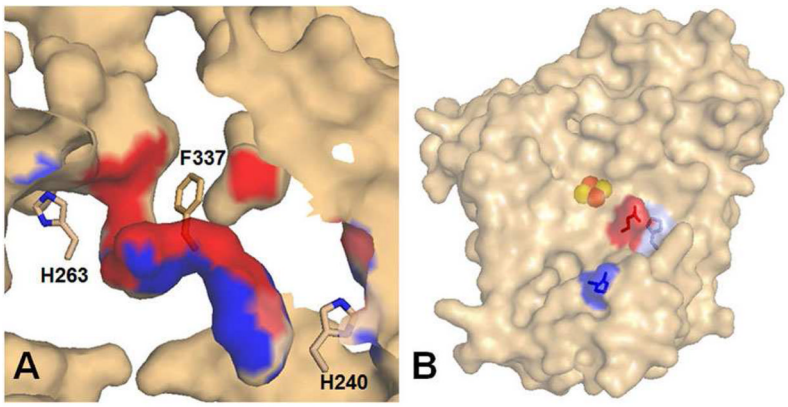

Figure 3. Channel and surface views of the H240 channel

Panel A shows the amphipathic nature of the H240 channel. Hydrophobic residues that contribute to the surface of this channel are shown in blue and polar residues in red. The catalytic histidine, H263, and residues F337 and H240 are shown as sticks and labeled. Panel B shows the surface representation of the matrix exposed face of the open conformation (PDB ID 2HRC) with residues H240 (light blue), R366 (dark blue) and E369 (red) shown as sticks.

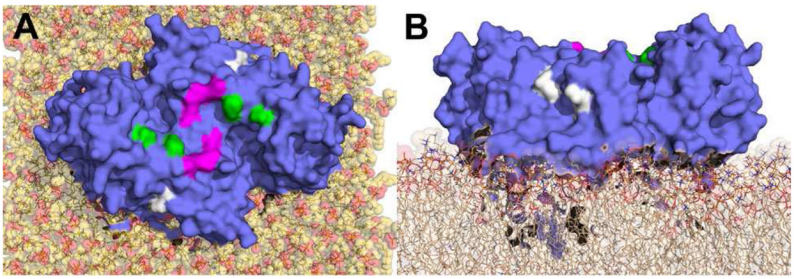

Figure 4. Location of surface residues on human ferrochelatase

Human ferrochelatase (PDB ID 2HRC) shown as as a slate surface representation is modeled into a lipid bilayer (tan or yellow sticks) (PDB DLPC_303K (49)). Surface patches representing the surface of the H240A channel (H240A, R366 and E369), cobalt binding residues (H231 and D383) and putative frataxin docking residues (E289 and R290) are shown in white, magenta and green, respectively. Panel A shows the enzyme surface from the matrix side of the inner mitochondrial membrane and Panel B shows a side profile of the enzyme embedded in the membrane.

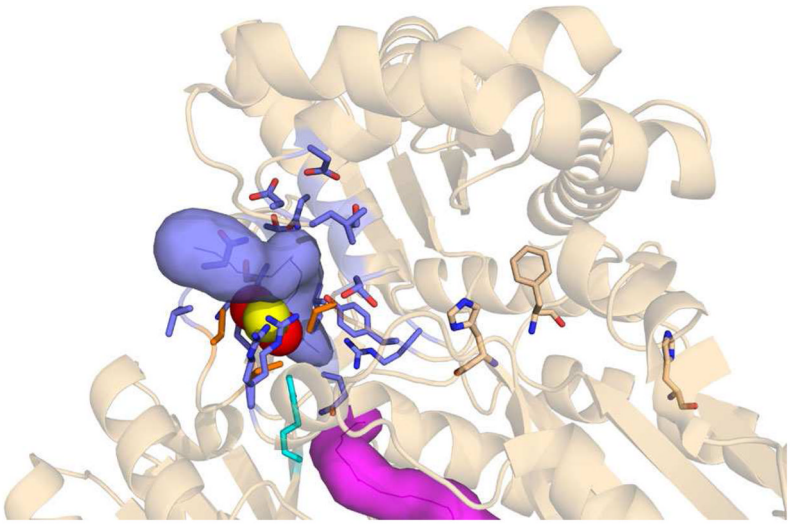

Figure 5. Cluster Channel. The cluster channel is shown in slate

Residues which contribute to the surface of the cluster channel are shown as sticks. For reference the dimer interface channel is shown in magenta, the active site residues H263 and F337 are shown as wheat sticks, residue R298 from the B subunit is shown in cyan and the four cysteine residues which serve as ligands for the [2Fe-2S] cluster are shown as orange sticks.

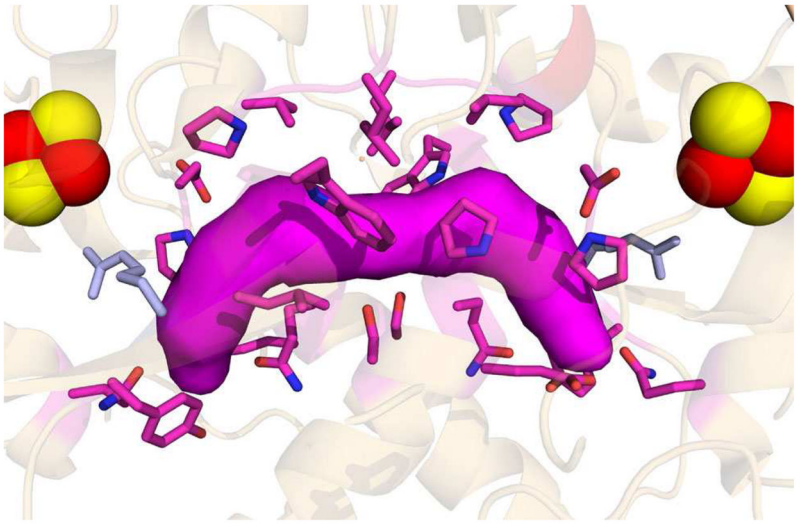

Figure 6. Dimer Interface Channel

The channel found at the dimer interface is shown in magenta. Residues from each subunit that contribute to the surface of this channel are shown as sticks and the [2Fe-2S] clusters from each subunit are shown as red and yellow spheres. The side chain of residue R298 from each subunit is shown as light blue sticks.

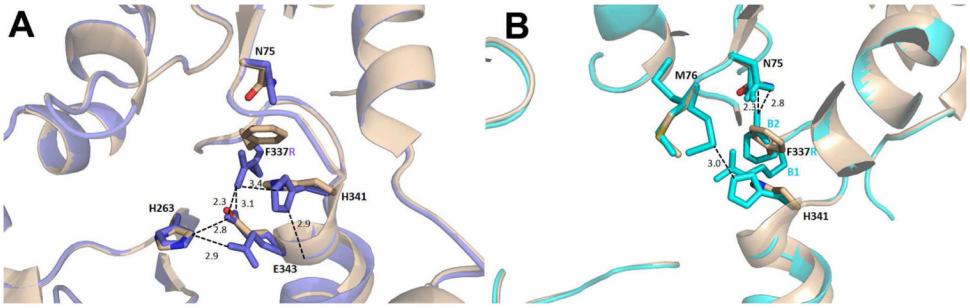

Figure 7. Comparison of the active site of the inactive variant F337R and wild-type ferrochelatase

Panel A shows the orientation of F337R in the A monomer and the B1 conformers in the B monomer and its interactions with residues in the bottom of the active site pocket of ferrochelatase. Hydrogen bonding interactions in the F337 variant are indicated with dashed lines and distance in Å shown. Wild-type active site residues are shown in wheat, blue, red and yellow for carbon, nitrogen, oxygen and sulfur atoms, respectively. Active site residues of the F337R variant are shown in slate. Panel B shows the orientations of F337R in the active site of the B monomer. Hydrogen bonding interactions from the B2 conformer of F337R with N75 in the top of the active site are indicated as described in panel A. The distance between H341 and one conformer of M76 in the F337R variant is also shown. Wild-type residues are shown as described in panel A and those of the B monomer of F337R are shown in cyan.

Table 1

Data collection and refinement statistics for variants of human ferrochelatase presented here.

Variant	H240A	F337R	F110A/S197C
Resolution Range (Å)	50.0-1.8(1.86)[a]	50.0-1.8(1.86)	50.0-2.5(2.59)
R_{sym} (%)[b]	8.2(28.1)	8.9(32.7)	8.7(22.7)
I/σ	38(4)	40(5)	11(2)
Redundancy	8(5)	9(6)	5(3)
Unique Reflections	163,439	165,727	30,208
R_{cryst} (%)	18.5	17.5	22.3
R_{free} (%)	22.3	21.7	28.0
RMSD Bonds (Å)	0.007	0.008	0.008
RMSD Angles (°)	1.3	1.34	1.4
Average B Factor	18.0	19.2	40.8
PDB ID	3AQI	4F4D	4F4G

[a] Numbers in parenthesis represent the lower resolution limit for the outer resolution shell.

[b] $R_{sym} = \Sigma_{hkl}[\Sigma_I(|I_{hkl,I} - \langle I_{hkl}\rangle|)]/\Sigma_{hkl,I}\langle I_{hkl}\rangle$, where I_{hkl} is the intensity of an individual measurement of the reflection with indices hkl and $\langle I_{hkl}\rangle$ is the mean intensity of that reflection.

TABLES. Each table must have a brief (one phrase or sentence) title that describes its contents.

Table 2

In vivo analysis of human ferrochelatase surface and active site variants

Heme synthesis values reported represent the average of heme content from three different experiments with <10% standard deviation.

Variant	Complementation of Δ*hem15*	Heme synthesis (% of wild type)
Y165F	Yes	56
H263C	No	--
R164L/Y165L	No	--
H240A	Yes	89
H240E	Yes	56
E369T	Yes	86
H240A/R366E	Yes	53
H240A/E369T	Yes	36
H231A/D383A	Yes	71
H231A/D383K	Yes	84
R290E	Yes	92
E289K	Yes	100
E289A/R290A	Yes	85

Table 3
Kinetic parameters for wild-type and variant human ferrochelatases

Values reported represent the average parameters determined from four separate experiments with <10% standard deviation.

Residue	K_m iron (μM)	K_m meso (μM)	k_{cat} (min^{-1})	Rescue Δ*hemH*
Wild-type (13)	18	28	4.2	Yes
R115L (13)	21	34	3.2	Yes
N75A (20)	33.8	16.8	0.96	Yes
I132A	ND	ND	ND	Yes
Q139A	ND	ND	ND	Yes
Q139L	26.2	26.7	0.60	Yes
S201A	8.4	13.2	1.8	Yes
F237Y	13.8	ND	0.8	Yes
F237L	16	14	1.4	Yes
H240A	27.6	12.1	3.42	Yes
H240E	21.1	12.6	2.8	Yes
H240K	27.9	17.9	4	Yes
I241F	21.5	11.3	1	Yes
Q302A	52.6	29.3	4.5	Yes
Q302D	--	--	--	Yes
V333A	ND	ND	ND	Yes
V333S	ND	ND	ND	Yes
P334L	48.8	18.2	0.56	Yes
F337A (20)	17.8	24.6	0.81	Yes
F337R	--	--	--	No
S339A	ND	ND	ND	Yes
T344A	25.9	20.1	0.65	Yes
T344K	--	--	--	No
A368C	16.8	51.9	3.28	Yes
A368F	--	--	--	Yes
A368L	18.1	36.9	0.94	Yes
S370A	39.7	11.4	3.1	Yes
S370C	40	33	3	Yes

ND not determined, -- not measurable